SUPPORTING INFORMATION

Dehalogenation of Polybrominated Diphenyl Ethers and Polychlorinated Biphenyl by Bimetallic, Impregnated and Nanoscale Zerovalent Iron

Yuan Zhuang[a], Sungwoo Ahn[a], Angelia L. Seyfferth[b], Yoko Masue-Slowey[b], Scott Fendorf[b] and Richard G. Luthy[a]*

a: Department of Civil and Environmental Engineering

b: Department of Environmental Earth System Science

Stanford University, Stanford, CA 94305-4020

(24 pages, 3 equations, 12 figures)

Nanoscale Zerovalent Iron (nZVI) and Palladized nZVI Synthesis Details.

800 ml of methanol/milli-Q water solution (30:70, v/v) containing 20 g ferrous sulfate ($Fe(SO_4)\cdot 7H_2O$, Fluka) was adjusted to pH 6.5 - 7 by adding 10 ml of 5N NaOH (ACS grade, EMD) solution dropwise. Next, 50 ml of sodium borohydride ($NaBH_4$, Sigma-Aldrich) solution (80 g/L) was added dropwise while stirring, resulting in a suspension of iron particles. nZVI particles were isolated by centrifugation in 760 ml size centrifuge tubes for 15 minutes at 2000 rpm, and the supernatant was discarded. For Pd doping, fresh nZVI particles were washed with 200 ml methanol to remove remaining $NaBH_4$, dispersed in 100 ml methanol, and mixed with 20 ml palladium acetate ($Pd(CH_3CO_2)_2$, 42.2 mg, Fisher) in methanol solution on a shaker (200 rpm) for 30 minutes. The wet nZVI and nZVI/Pd particles obtained after decanting the overlying solution were rinsed with methanol, frozen at -80 °C over 2 hours, and then dried using a vacuum freeze-drier (VirTis Freezemobile 12ES, SP industries inc., Gardiner, NY) for 2 days. Nitrogen (99.98% purity) was purged into the freeze dryer after drying and the tubes were capped immediately afterwards to minimize exposure to the atmosphere. The dried nZVI particles were transferred to a glove box (Labconco Corporation, Kansas City, MO) filled with N_2, ground into fine powder using a spatula, and stored in glass vials prior to use.

Activated Carbon Impregnated Palladized nZVI Syntheis Detail.

Granular activated carbon (HD 3000, Norit Americas Inc.) was washed by boiling in water twice, and dried in oven at 105°C overnight. AC was sieved with a no. 30 sieve to remove grains smaller than 0.595 mm. Iron is incorporated into the AC via an incipient wetness impregnation method, where 22.8 g of $Fe(NO_3)_3\cdot 9H_2O$ (ACROS) was melted at 55-60°C with a small quantity of water (5 mL) and then mixed with 10 g of AC for 10 min. For total incorporation of Fe to the AC, the slurry was dried at room temperature, put in an oven at 105°C overnight and further calcined in a furnace (Thermolyne 48000, Dubuque, IA) at 300°C to remove nitrate ions, held for 4 h, and allowed to cool down naturally. Unincorporated free Fe was removed using a no. 30 sieve (Fe-AC, the Fe is iron oxide). 4 g Fe-AC was resuspended in 50 mL of methanol/DI water (30/70, v/v), the pH adjusted to 6.5-7.0 by adding a 5 N NaOH solution drop by drop. A 20 mL aqueous solution of 1.6 g $NaBH_4$ (Sigma-Aldrich) was prepared to reduce Fe(III) to elemental Fe. The mixture was stirred until no significant H_2 production was observed (~3 h). Then the AC composite was recovered by filtering the slurry with a no. 30 sieve, washed with copious amounts of methanol to remove free ZVI and other impurities (nZVI-AC). For Pd doping, 42.2 mg $Pd(CH_3CO_2)_2$ (Fisher) was dissolved in 50 ml of methanol for 2 h. Then fresh nZVI-AC particles were washed with methanol, immersed into a Pd solution, and stirred for 30 min. The wet particles

were frozen at -80°C over 2 hours, and freeze dried (Vistil Freezemobile 12ES) for 2 days. Nitrogen (99.98% purity) was purged into freeze dryer at the end to minimize the exposure to air, before transfer into glove box. The particles were passivated by exposing them in glove box overnight, ground and stored in the glove box for later use (nZVI/Pd-AC). At the end of each procedure, samples are sieved with a no. 30 sieve to remove grains smaller than 0.595 mm.

Micro X-ray Fluorescence (μXRF) Imaging and Micro X-ray Absorption Spectroscopy (μXAS).

Elemental distributions of Fe and Pd, as well as species distributions of Fe^0 and Fe^{3+} were obtained on a thin section (30 μm) of a nZVI/Pd-AC particle by micro X-ray fluorescence (μXRF) imaging and micro X-ray absorption spectroscopy (μXAS) on beam line 10.3.2. at the Advanced Light Source at Lawrence Berkeley National Laboratory, after embedment in epoxy (EPO-TEK 301 2FL). This bend magnet beamline uses a double crystal (Si 111) monochromator and K-B mirrors to deliver microfocused X-rays of 5 x 5 μm spot size. The sample, mounted on a quartz slide, was mounted onto an aluminum sample holder placed at 45˚ to the incident beam. The monochromator was calibrated using a Fe foil, which was assigned its first inflection point at 7112 eV. Utilizing 7 μm step size and 50 ms dwell time per pixel, fluorescence intensities of Fe and Pd were monitored with a seven element Ge solid-state detector placed 45˚ to the sample (90˚ to the incident beam). For Fe speciation, the sample was imaged at three energies 8000, 7111.25, and 7100 eV to create images of total Fe, Fe^{3+}, and Fe^0, respectively. A least squares combination fitting of those three energies to the normalized intensities from the standards of ferric nitrate and zero valent iron was conducted. The distribution of Pd was obtained by further imaging the sample at 3190 and 3167 eV, and subtracting the image at 3167 to remove background interference from Ar, Cl, and K.

Sample Extraction and Analysis.

The whole nZVI and nZVI/Pd samples were extracted three times using 3 mL toluene (for PBDEs) or hexane (for PCB 21). For nZVI/Pd-AC tests, whole samples were centrifuged at 2000 rpm for 10 min. The liquid phase was carefully separated into 40 mL vials (volume measured), and extracted twice with 3 mL toluene. The collected extract for each liquid sample was dried using anhydrous Na_2SO_4 (granular, 10 – 60 mesh, Fisher), and further concentrated down to 1 mL under a gentle N_2 stream. The solid part of nZVI/Pd-AC was dried under a nitrogen evaporator for 30 minutes and extracted with 150 mL toluene using a soxhlet apparatus for 22 hours, macro-concentrated by a heating

mantle to 30 mL, and micro-concentrated to 1 mL by a nitrogen evaporator in a water bath (EPA method 1614). Extracts were cleaned with a florisil (PR, Fluka) column, eluted with 20 mL methylene chloride:hexane (50/50, v/v), and then concentrated to 1 mL.

PCB 15 (Ultra scientific), an internal standard for PBDEs, or PCB 30 (Ultra scientific), an internal standard for PCB, was spiked into each sample prior to analyses for quantification purposes. PBDEs in the extracts were analyzed using gas chromatography with mass spectrometric detector (GC-MSD, Agilent 6890N-5973N, Palo Alto, CA) equipped with a HP-5ms capillary column (30.0 m × 250 μm × 0.25 mm) as described previously (1). PCBs in the extracts were analyzed by gas chromatography with electron-capture detector (GC-ECD, Agilent 6890, Palo Alto, CA) equipped with a HP-5 fused silica capillary column (60.0 m × 250 μm × 0.25 mm) (2).

Equation S1. Pseudo-first-order dehalogenation kinetic expression.

$$\ln\left(\frac{C}{C_O}\right) = -k_{obs}t$$

C and C_0 denote the concentrations of parent compounds at any sampling and initial time, respectively. k_{obs} is the observed first-order rate constant [1/d], and t is reaction time [d].

Equation S2. Based on sequential debromination of BDE 12 shown in the scheme below, the rate equations of BDE 12 and its debrominated products can be expressed as follows (1 denotes BDE 12; 2 denotes BDE 2; 3 denotes BDE 3; 4 denotes diphenyl ether).

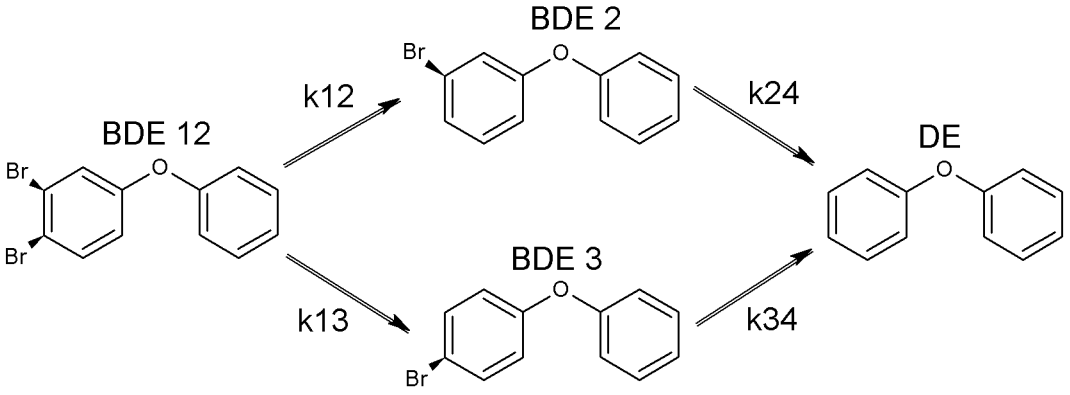

$$\frac{dC_1}{dt} = -\left(k_{12} + k_{13}\right)C_1$$

$$\frac{dC_2}{dt} = k_{12}C_1 - k_{24}C_2$$

$$\frac{dC_3}{dt} = k_{13}C_1 - k_{34}C_3$$

$$\frac{dC_4}{dt} = k_{24}C_2 + k_{34}C_3$$

With initial conditions, at $t = 0$

$$C_1 = C$$

$$C_2 = C_3 = C_4 = 0$$

Analytical solutions for those equations are as follows (α denotes the fraction of the moles of a certain BDE normalized by the initial moles of BDE 12):

$$\alpha_1 = e^{-(k_{12}+k_{13})t}$$

$$\alpha_2 = \frac{k_{12}}{k_{24} - (k_{12} + k_{13})}\left[e^{-(k_{12}+k_{13})t} - e^{-k_{24}t}\right]$$

$$\alpha_3 = \frac{k_{13}}{k_{34} - (k_{12} + k_{13})}\left[e^{-(k_{12}+k_{13})t} - e^{-k_{34}t}\right]$$

$$\alpha_4 = \frac{k_{24}k_{12}}{k_{24} - (k_{12} + k_{13})}\left[\frac{e^{-(k_{12}+k_{13})t} - 1}{-(k_{12} + k_{13})} - \frac{e^{-k_{24}t} - 1}{-k_{24}}\right] + \frac{k_{34}k_{13}}{k_{34} - (k_{12} + k_{13})}\left[\frac{e^{-(k_{12}+k_{13})t} - 1}{-(k_{12} + k_{13})} - \frac{e^{-k_{34}t} - 1}{-k_{34}}\right]$$

Equation S3. Based on concerted (i.e., simultaneous) debromination of BDE 12 where BDE 12 can be directly debrominated to DE shown in the scheme below, the rate equations of BDE 12 and its debrominated products can be expressed as follows (1 denotes BDE 12; 2 denotes BDE 2; 3 denotes BDE 3; 4 denotes diphenyl ether).

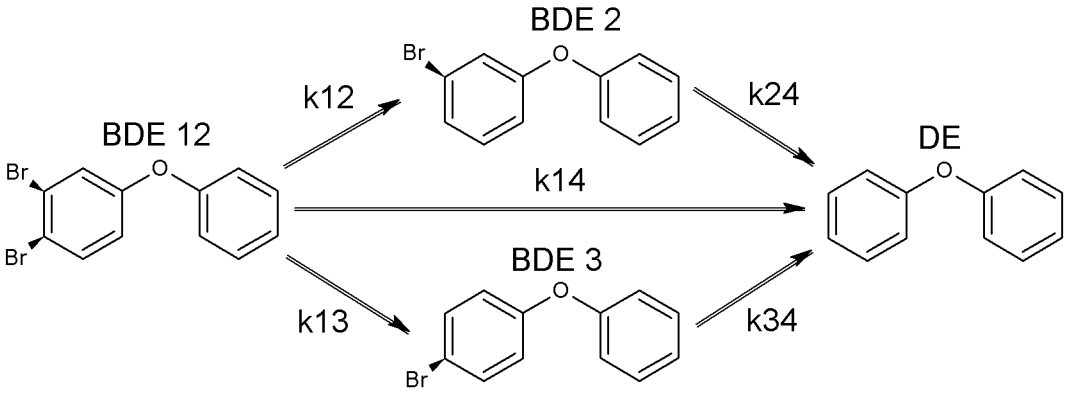

$$\frac{dC_1}{dt} = -(k_{12} + k_{13} + k_{14})C_1$$

$$\frac{dC_2}{dt} = k_{12}C_1 - k_{24}C_2$$

$$\frac{dC_3}{dt} = k_{13}C_1 - k_{34}C_3$$

$$\frac{dC_4}{dt} = k_{24}C_2 + k_{34}C_3 + k_{14}C_1$$

With initial conditions, at $t = 0$

$$C_1 = C$$

$$C_2 = C_3 = C_4 = 0$$

Analytical solutions for those equations are as follows (α denotes fraction of the moles of a certain BDE normalized by the initial moles of BDE 12):

$$\alpha_1 = e^{-(k_{12}+k_{13}+k_{14})t}$$

$$\alpha_2 = \frac{k_{12}}{k_{24}-\left(k_{12}+k_{13}+k_{14}\right)}\left[e^{-(k_{12}+k_{13}+k_{14})t} - e^{-k_{24}t}\right]$$

$$\alpha_3 = \frac{k_{13}}{k_{34}-\left(k_{12}+k_{13}+k_{14}\right)}\left[e^{-(k_{12}+k_{13}+k_{14})t} - e^{-k_{34}t}\right]$$

$$\alpha_4 = \frac{k_{24}k_{12}}{k_{24}-\left(k_{12}+k_{13}+k_{14}\right)}\left[\frac{e^{-(k_{12}+k_{13}+k_{14})t}-1}{-\left(k_{12}+k_{13}+k_{14}\right)} - \frac{e^{-k_{24}t}-1}{-k_{24}}\right]$$
$$+ \frac{k_{34}k_{13}}{k_{34}-\left(k_{12}+k_{13}+k_{14}\right)}\left[\frac{e^{-(k_{12}+k_{13}+k_{14})t}-1}{-\left(k_{12}+k_{13}+k_{14}\right)} - \frac{e^{-k_{34}t}-1}{-k_{34}}\right]$$

Figure S1. Transmission electron microscopy (TEM) images of nZVI/Pd particles. (a) Chain of nZVI/Pd particles. (b) Cluster of nZVI/Pd particles. nZVI/Pd particles tend to aggregate. No isolated Pd particles were observed. Palladization of nZVI did not affect the core-shell morphology as indicated in our previous study (1).

(a)

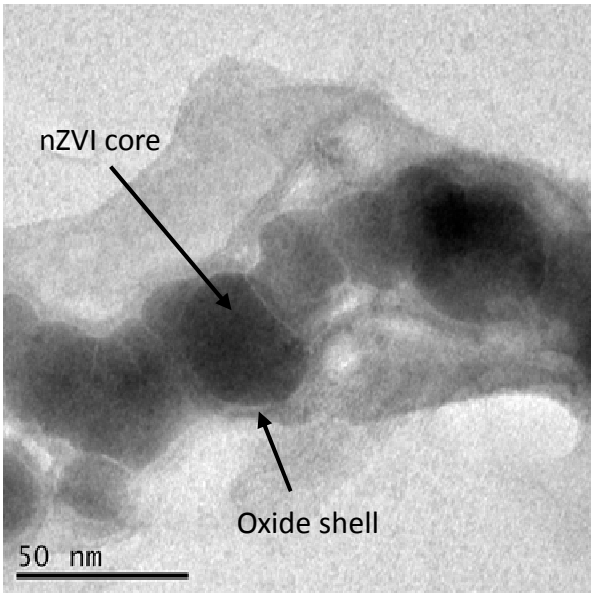

(b)

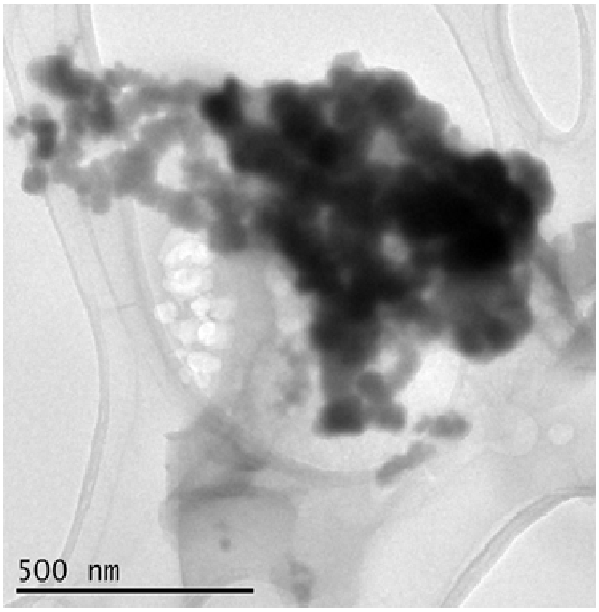

Figure S2. Iron composition analysis for nZVI/Pd-AC particles. (a) Surface and after sputtering, Fe2p3 spectrum from X-ray Photoelectron Spectroscopy (XPS). (b) Iron composition change with depth derived from Fe2p3 spectrum.

(a)

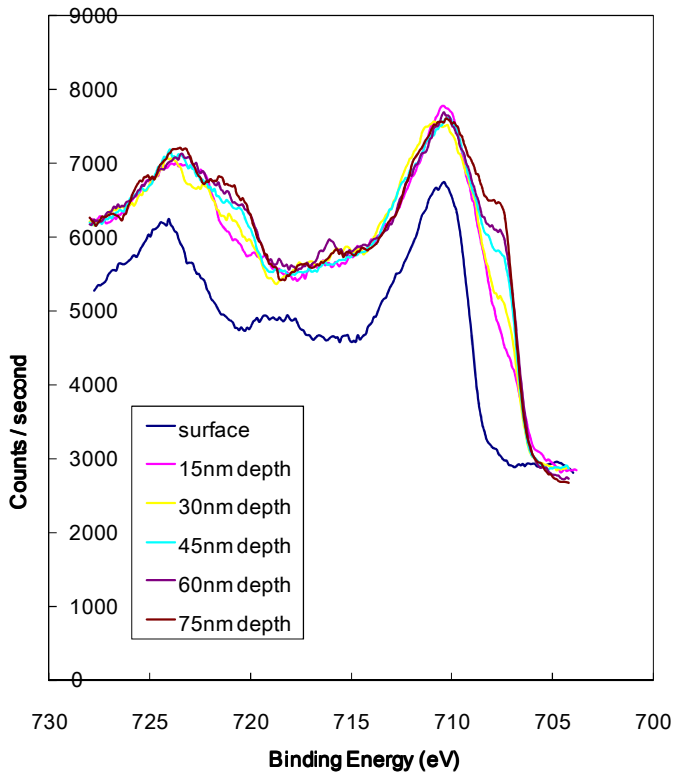

(b)

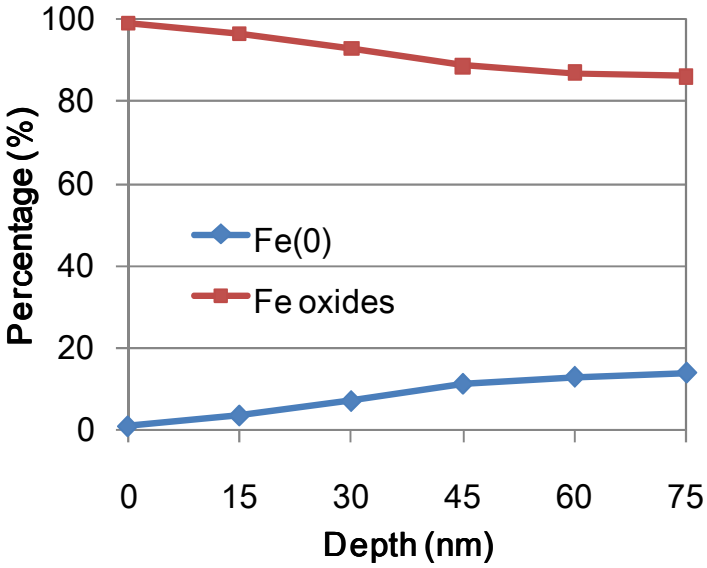

Figure S3. Pd3d spectra from X-ray Photoelectron Spectroscopy (XPS) for nZVI/Pd-AC surface and in depth by sputtering. Binding energies of 340.3 eV (Pd $3d_{3/2}$) and 335.0 eV (Pd $3d_{5/2}$) indicate that Pd is in the zero-valent form.

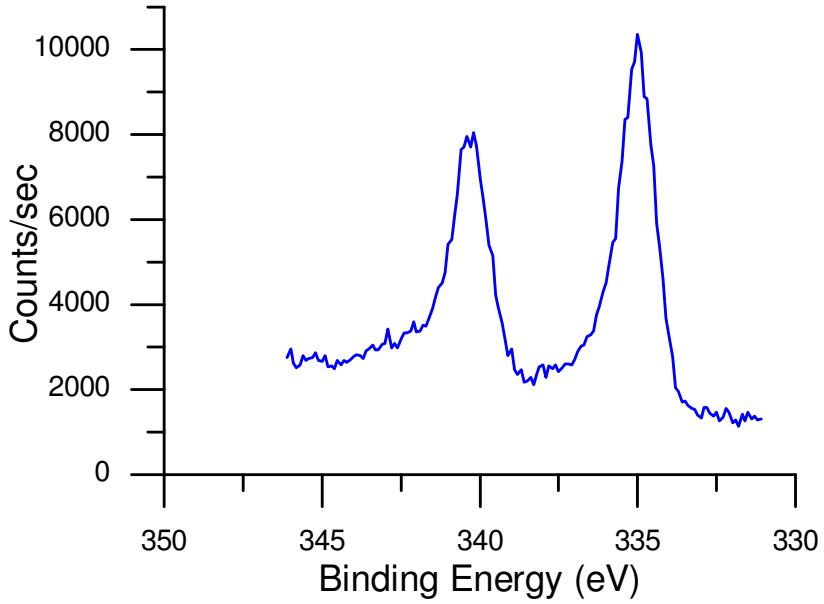

Figure S4. Degradation of selected BDEs by nZVI/Pd and changes in byproducts formation. The solid lines shown here are to visualize the trends of the data and do not represent the regression of the data. (a) BDE 21; (b) BDE 28; (c) BDE 33; (d) BDE 8; (e) BDE 12; (f) BDE1; (g) BDE 2; (h) BDE 3.

Note for Figure S4(a):
In the tests with BDE 21, a main peak comes out at a different residence time from those standards of indentified intermediates produced by stepwise debromination. This unidentified peak has the same main m/z pieces (168 and 328) as di-BDE, and shows a larger percentage of 168 m/z, consistent with di-BDEs with bromines at the ortho-position. From our previous test of BDE 5 with nZVI, an unusual shift of bromine to para- position was observed. Therefore, there is a possibility that this unidentified peak is a byproduct formed by a shift of bromine. In order to identify this peak, standards for di-BDEs with similar 168:328 m/z ratios and range of residence times, including BDE 8 (2,4'-diBDE), 9 (2,5-diBDE), 10(2,6-diBDE), were tested, but none has exactly the same residence time as the unidentified peak. As configuration might affect the polarity of a compound and thus the residence time on GC column, it is also possible that this unidentified intermediate is a stereoisomer for a di-BDE standard with ortho-bromines. Due to its persistence for debromination, we would assume that it is a stereoisomer for BDE 10.

(a) BDE 21

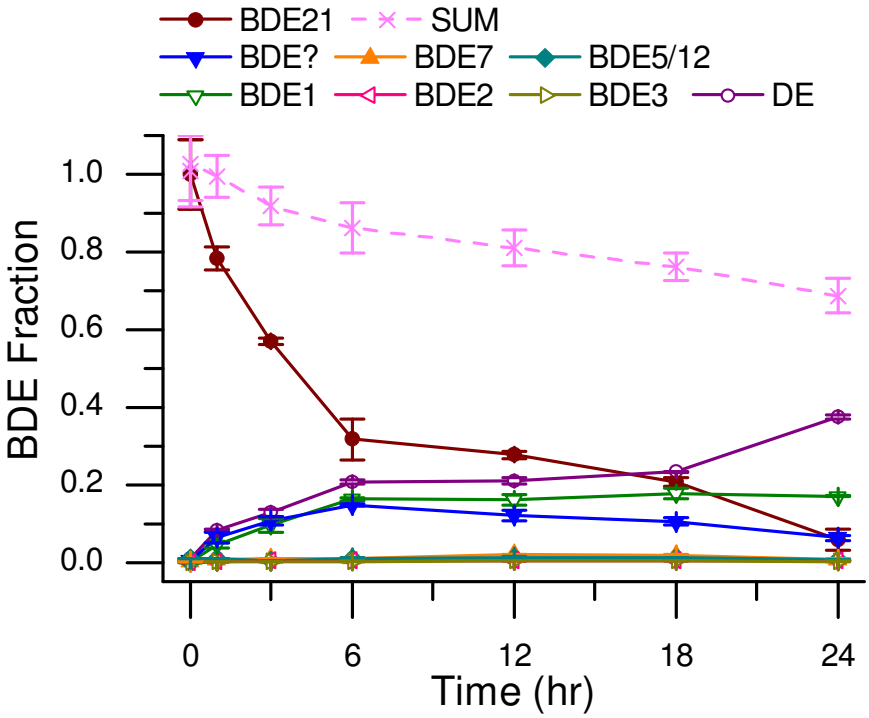

(b) BDE 28

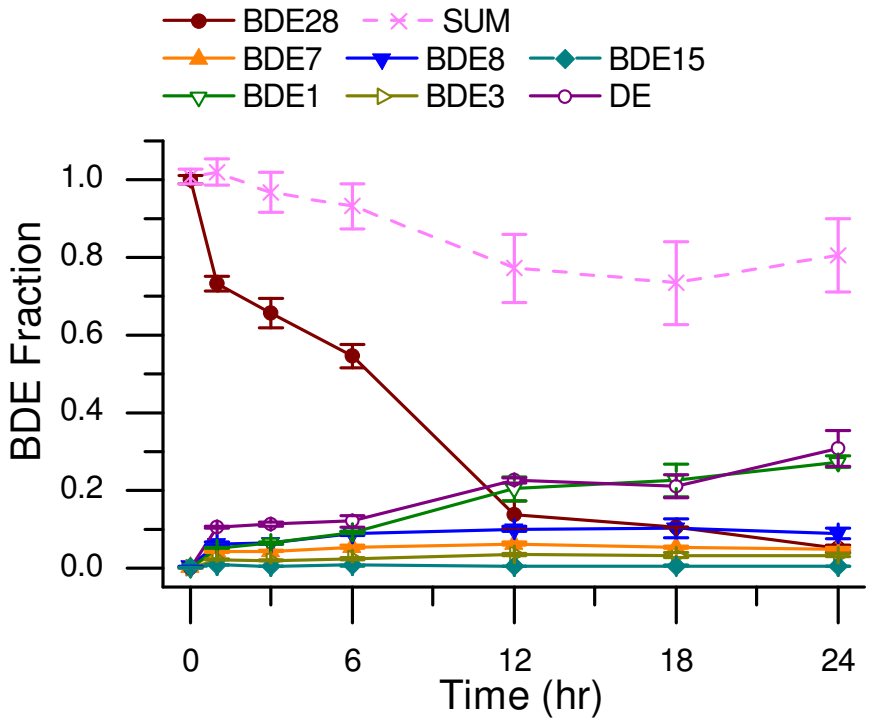

(c) BDE 33

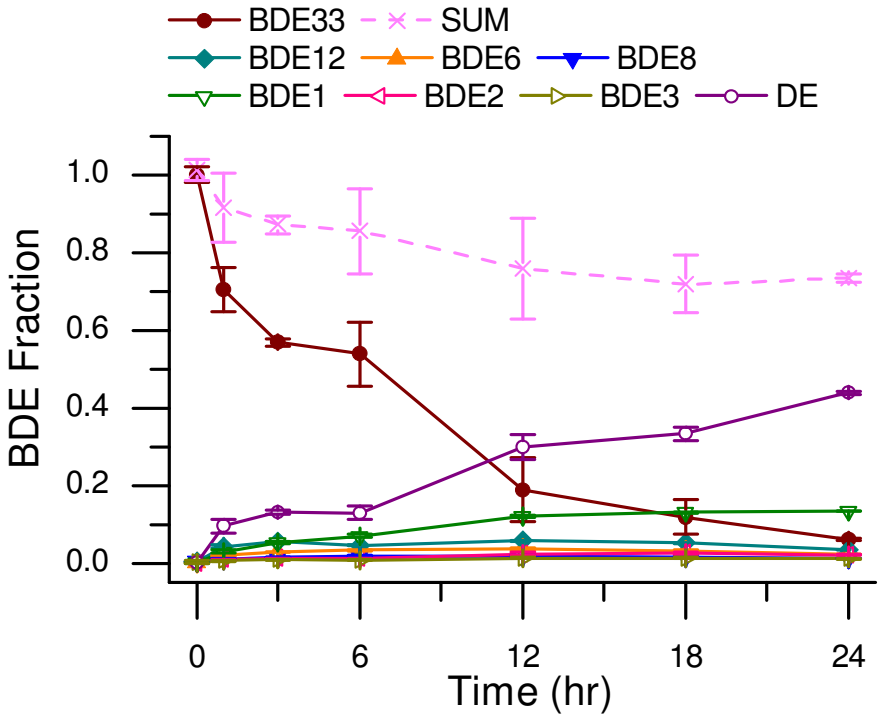

(d) BDE 8

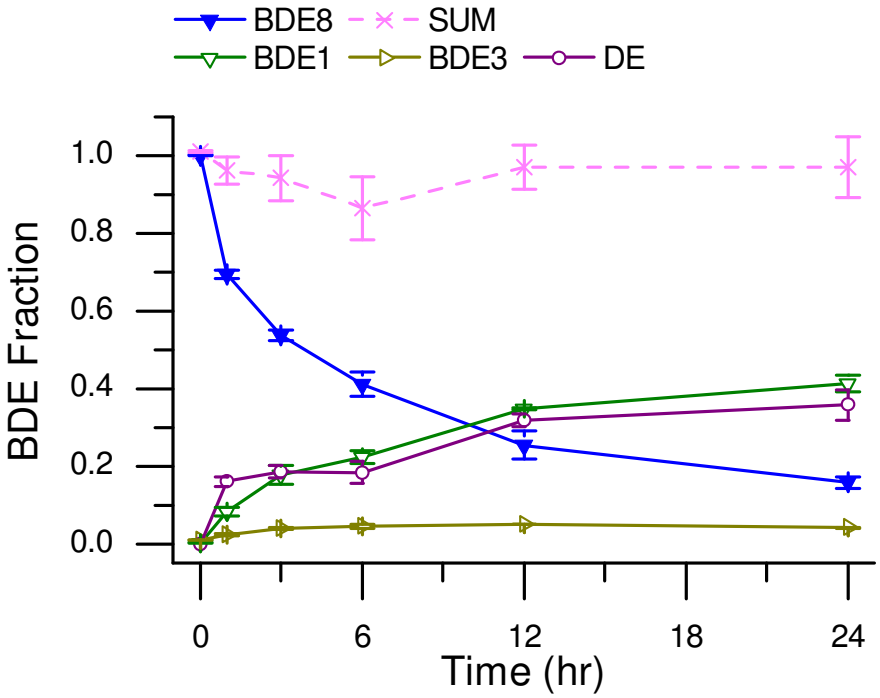

(e) BDE 12

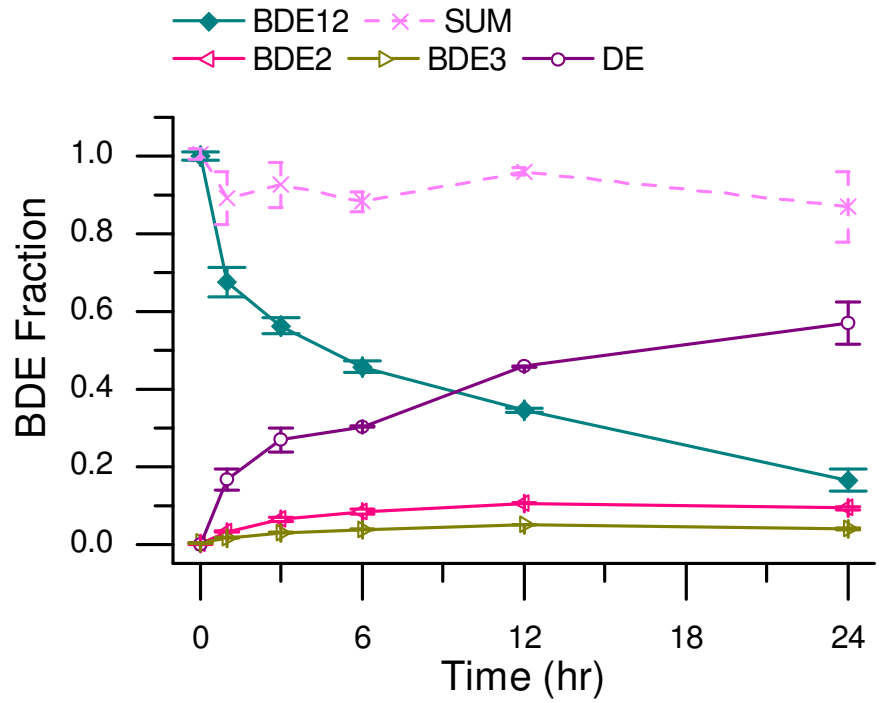

(f) BDE 1

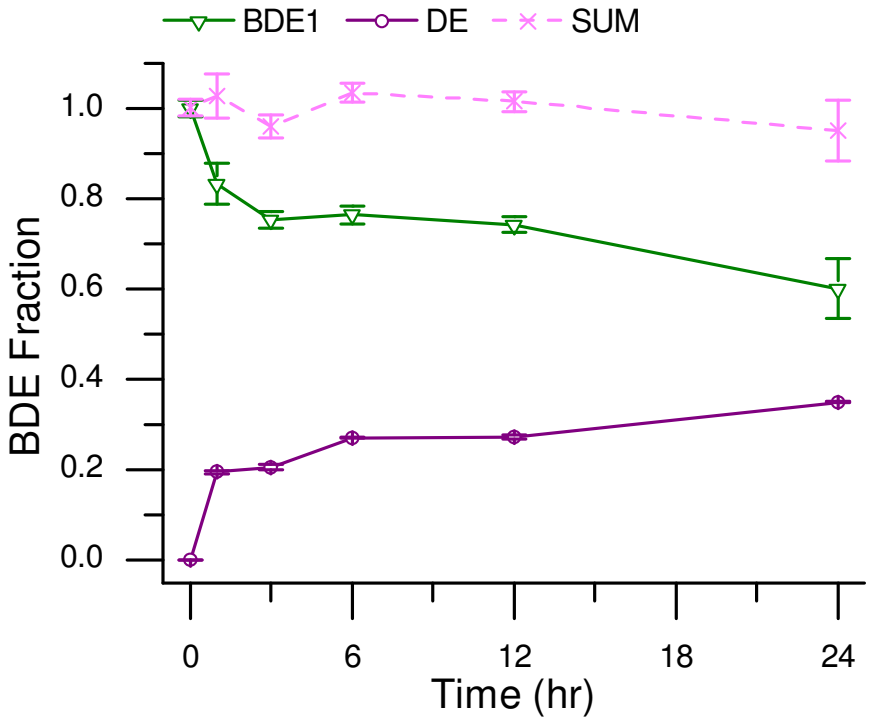
BDE1
DE
SUM
BDE Fraction
1.0
0.8
0.6
0.4
0.2
0.0
0
6
12
18
24
Time (hr)

(g) BDE 2

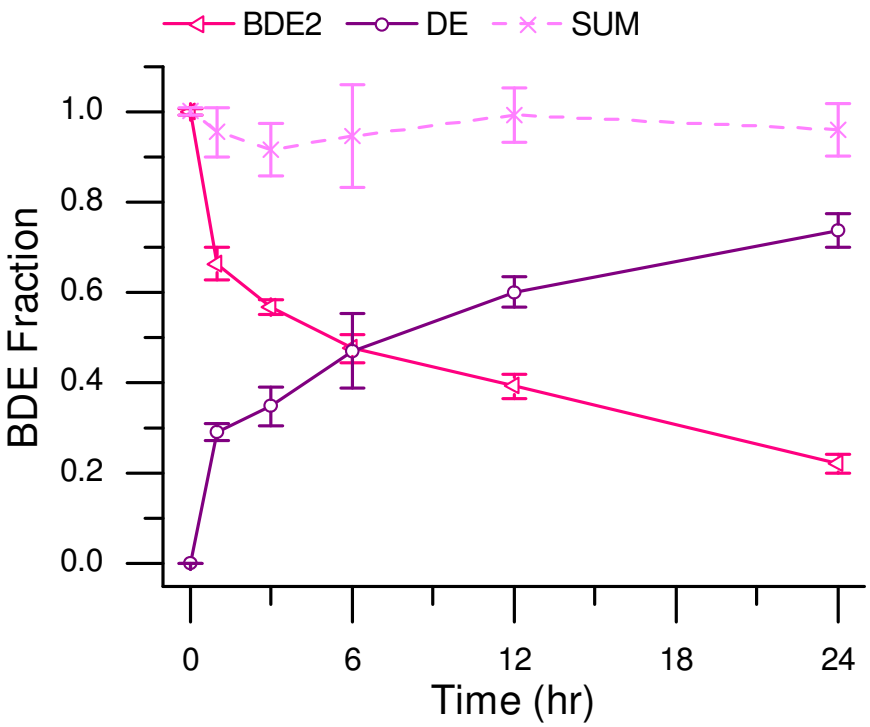
BDE2
DE
SUM
BDE Fraction
1.0
0.8
0.6
0.4
0.2
0.0
0
6
12
18
24
Time (hr)

(h) BDE 3

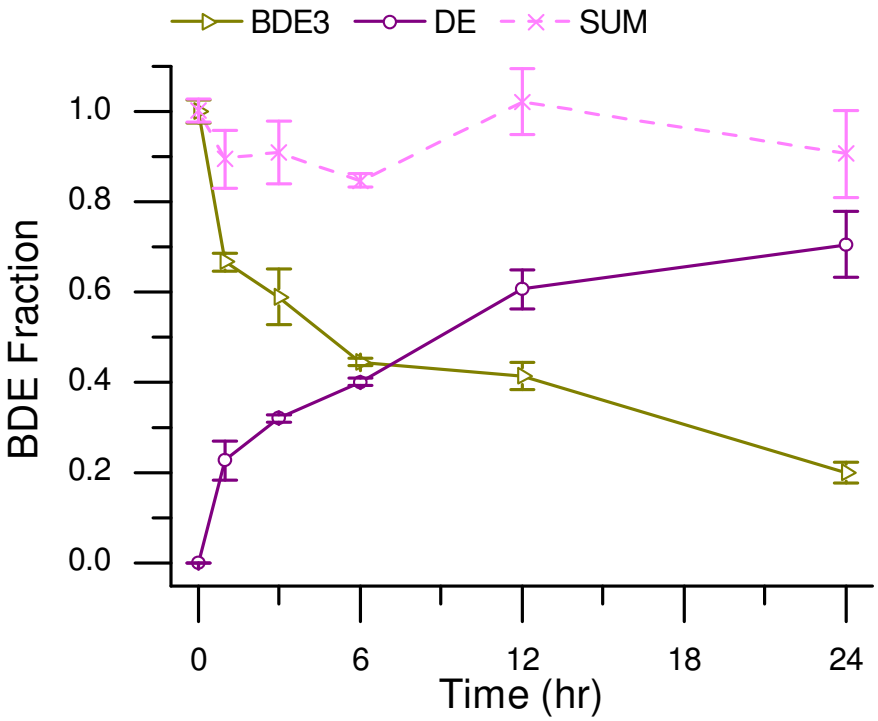

Figure S5. Correlations between observed debromination rate constants, k_{obs}, and (a) heat of formation, H_f, and (b) energy for the lowest unoccupied molecular orbital, E_{LUMO}. (The values of H_f and E_{LUMO} of BDEs were obtained from Hu et al. (3))

(a)

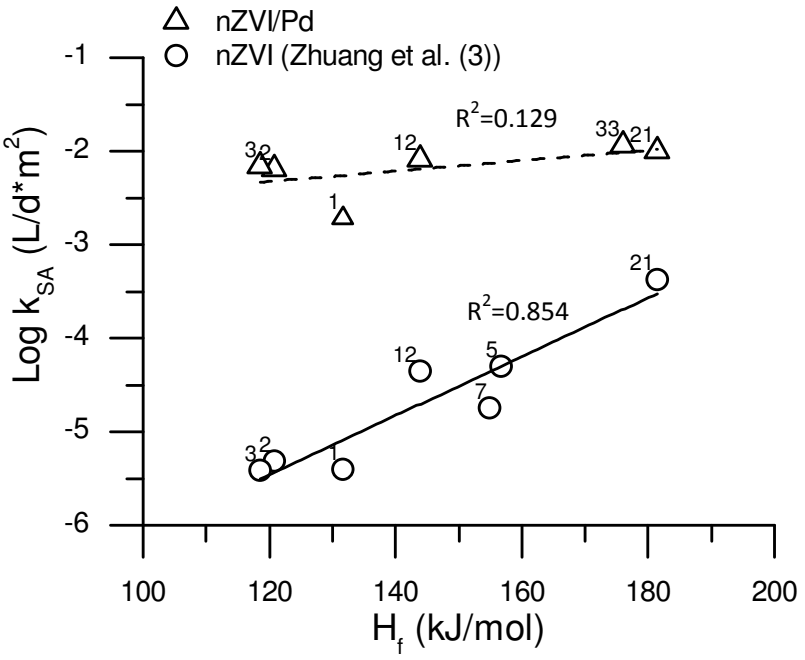

(b)

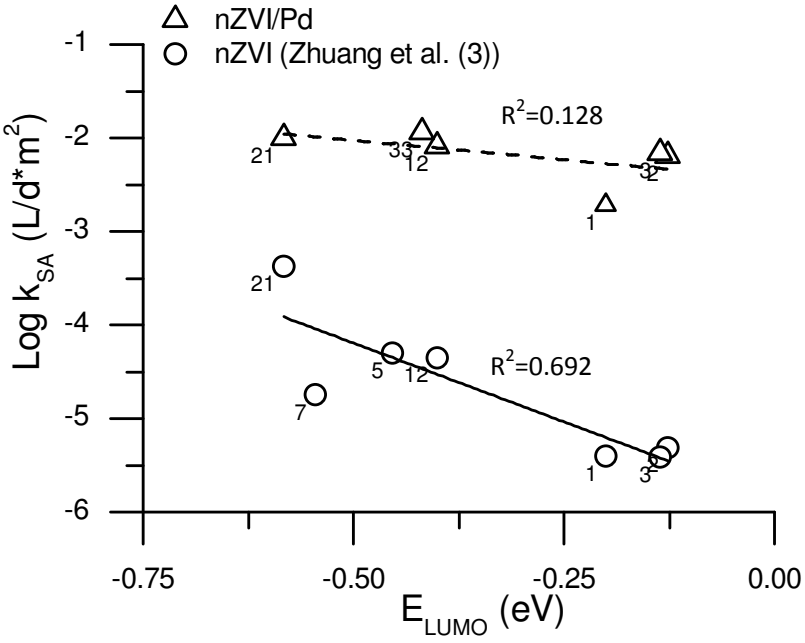

Figure S6. pH change during debromination of PBDEs by nZVI/Pd.

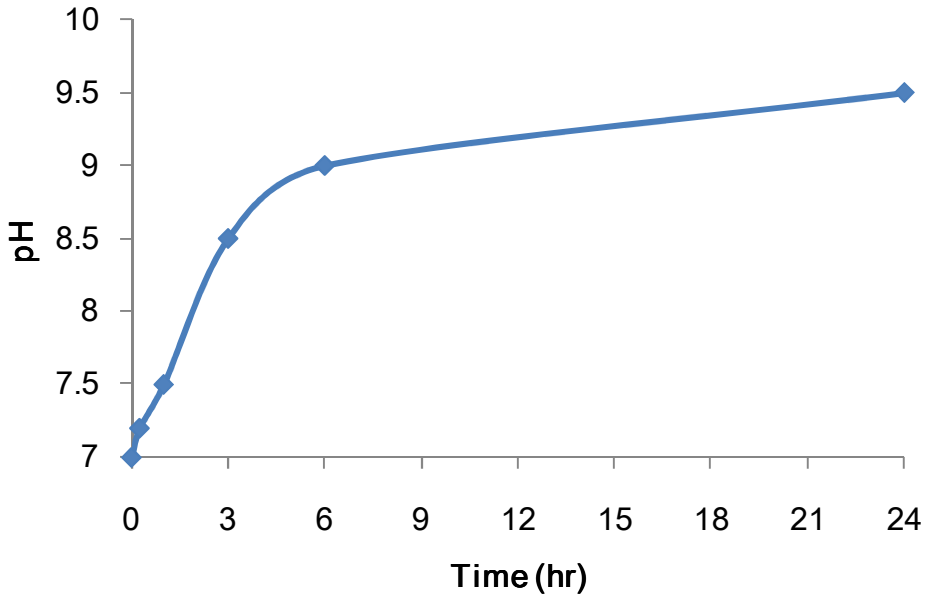

Figure S7. Degradation of BDEs by nZVI and changes in byproduct formation. The y-axis represents the mole fraction of a certain BDE normalized by the initial moles of the parent BDE. The data were fitted by assuming the reaction is pseudo-first order. (a) BDE 12, assuming sequential debromination pathways (Eq. S2), debromination rate constants for BDE 2 and BDE 3 are those in Table 2. (b) BDE 12, assuming sequential debromination pathway (Eq. S2), debromination rate constants for BDE 2 and BDE 3 are 3 times those in Table 2 because of activation. (c) BDE 12, assuming a concerted debromination pathway (Eq. S3), debromination rate constants for BDE 2 and BDE 3 are those in Table 2. (d) BDE 8, assuming a sequential debromination pathway (Eq. S2), debromination rate constants for BDE 1 and BDE 3 are those in Table 2. (e) BDE 8, assuming a sequential debromination pathway (Eq. S2), debromination rate constants for BDE 1 and BDE 3 are 3 times of those in Table 2 because of activation. (f) BDE 8, assuming a concerted debromination pathway (Eq. S3), debromination rate constants for BDE 1 and BDE 3 are those in Table 2.

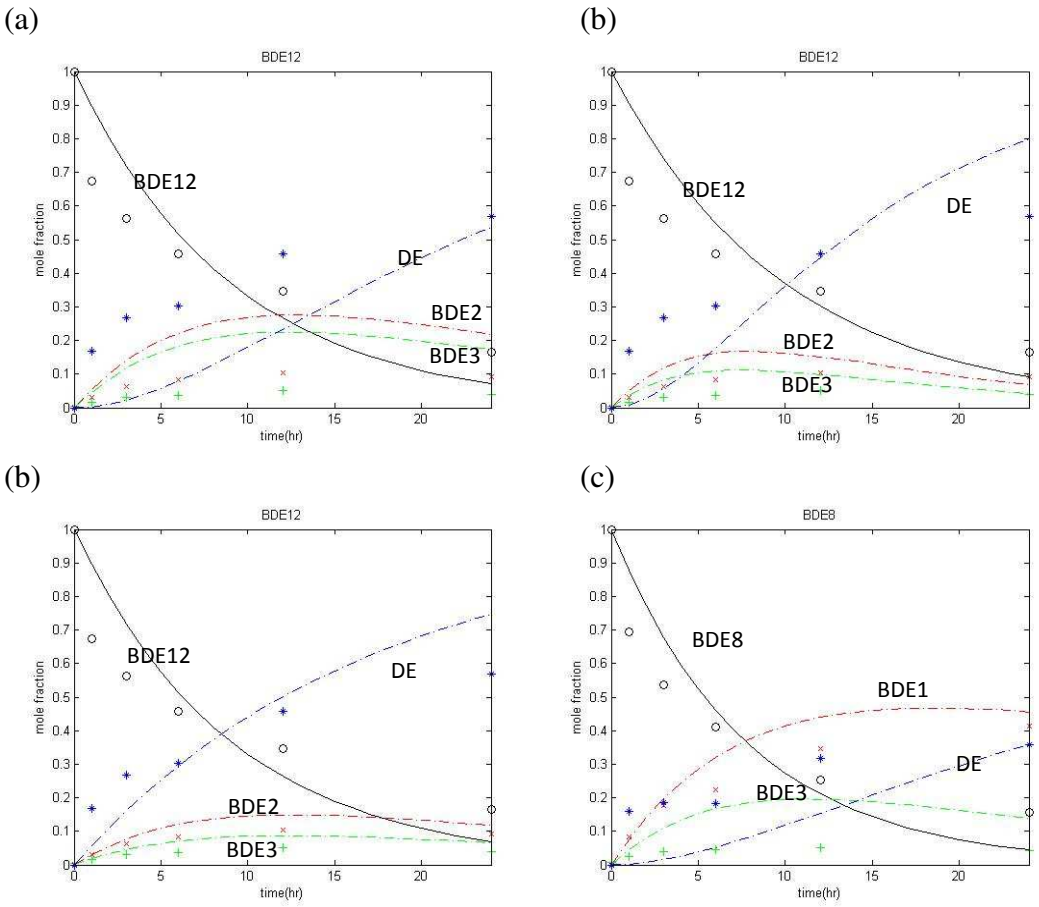

(e)

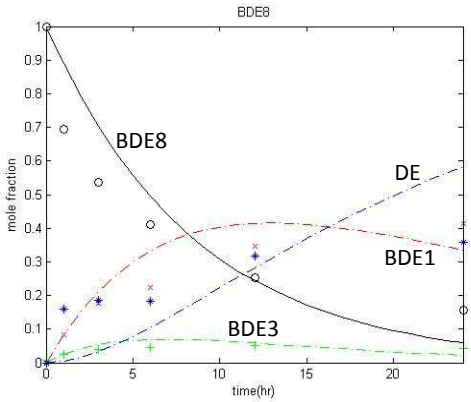
BDE8
BDE8
DE
BDE1
BDE3
mole fraction
time(hr)

(f)

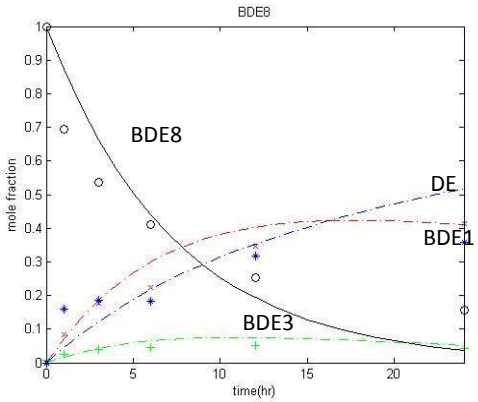
BDE8
BDE8
DE
BDE1
BDE3
mole fraction
time(hr)

Figure S8. Dechlorination of PCB21 and changes in byproducts formation by (a) nZVI, (b) nZVI/Pd. The solid lines shown here are to visualize the trends of the data and do not represent the regression of the data.

(a)

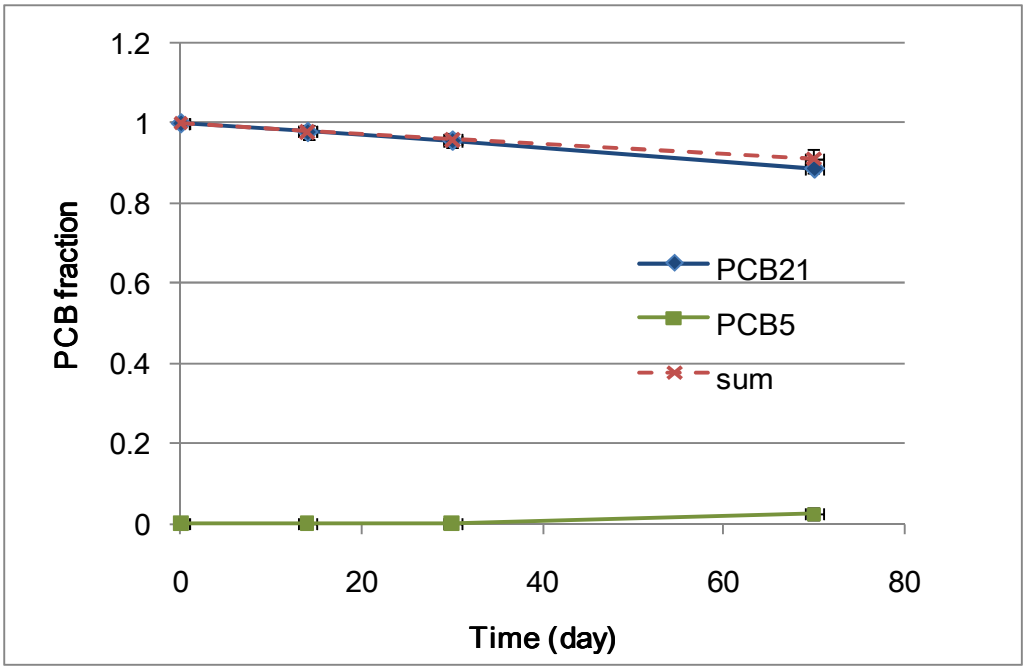

(b)

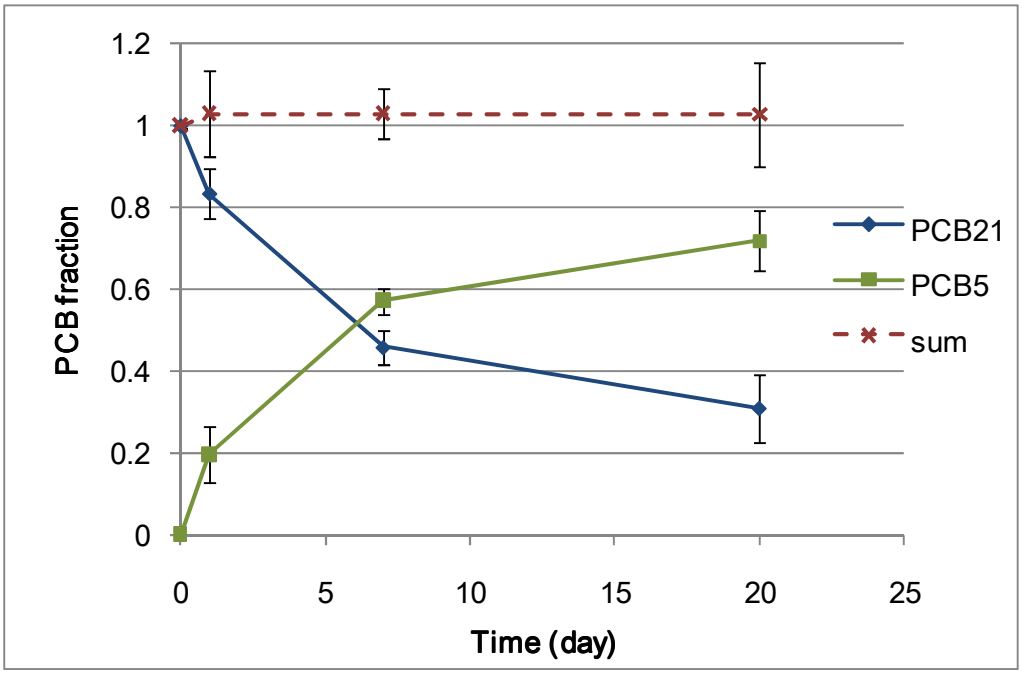

Figure S9. Debromination of BDE21 by nZVI/Pd-AC. The Y-axis represents the fraction of a certain BDE normalized by the initial moles of BDE 21. (a) Detected BDE 21 and products; (b) Adjusted data assuming the percentage of each compound in the unextracted portion of solid phase is the same as that observed from the extracted portion; (c) Detailed byproducts distribution after adjustment.

(a)

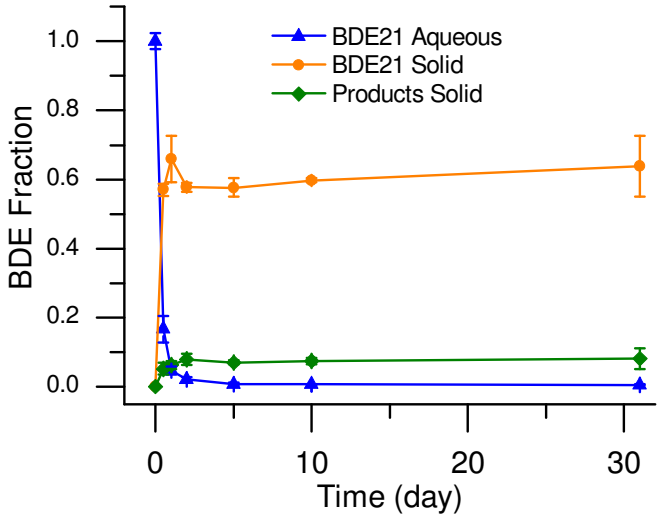

(b)

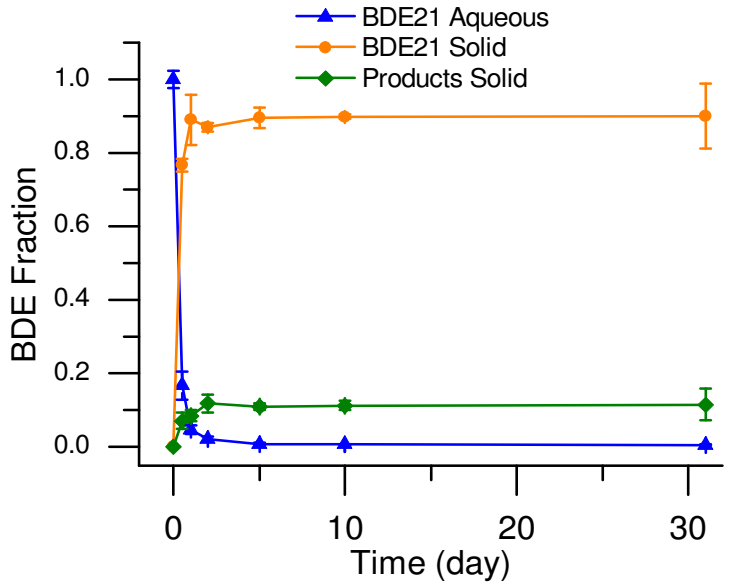

(c)

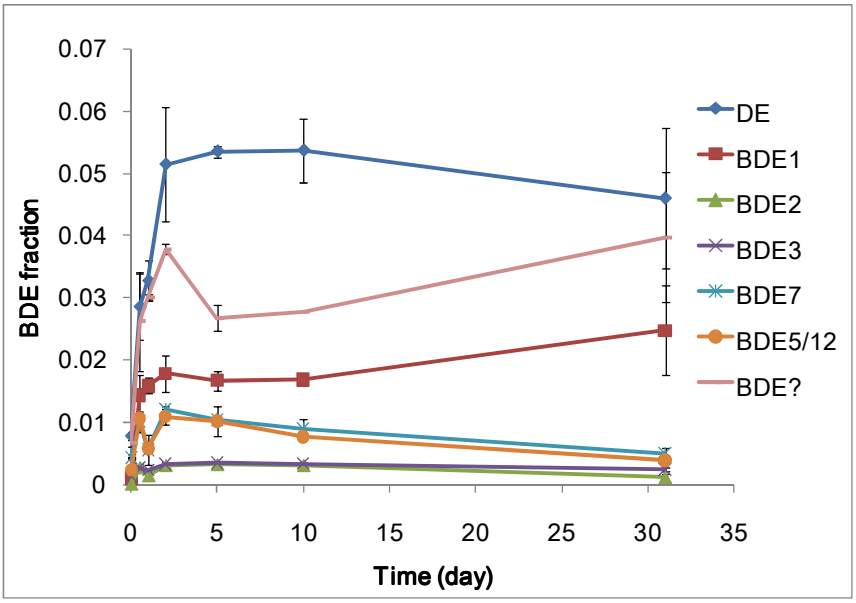
0.07
0.06
0.05
0.04
0.03
0.02
0.01
0
BDE fraction
0
5
10
15
20
25
30
35
Time (day)
DE
BDE1
BDE2
BDE3
BDE7
BDE5/12
BDE?

Figure S10. Sorption and debromination reaction scheme for BDE on nZVI/Pd-AC

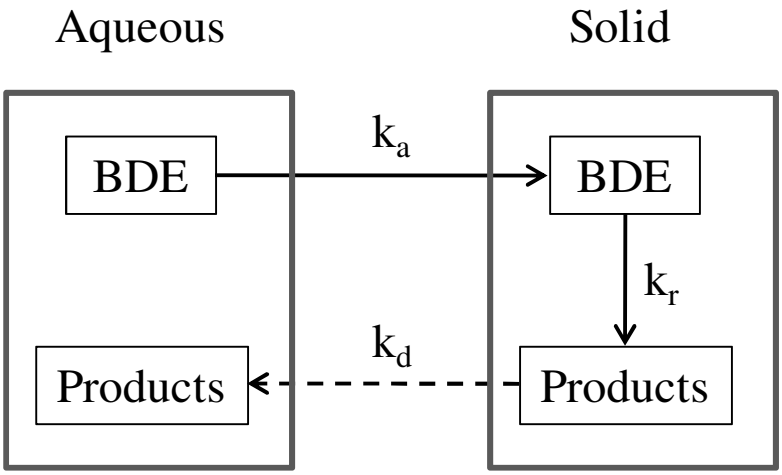

Figure S11. Effect of exposure to 10 ml acetone/water (50:50, v/v) solution on nZVI fraction in nZVI/Pd-AC. The Y-axis represents the fraction of the moles of nZVI normalized by the initial moles of nZVI in the system.

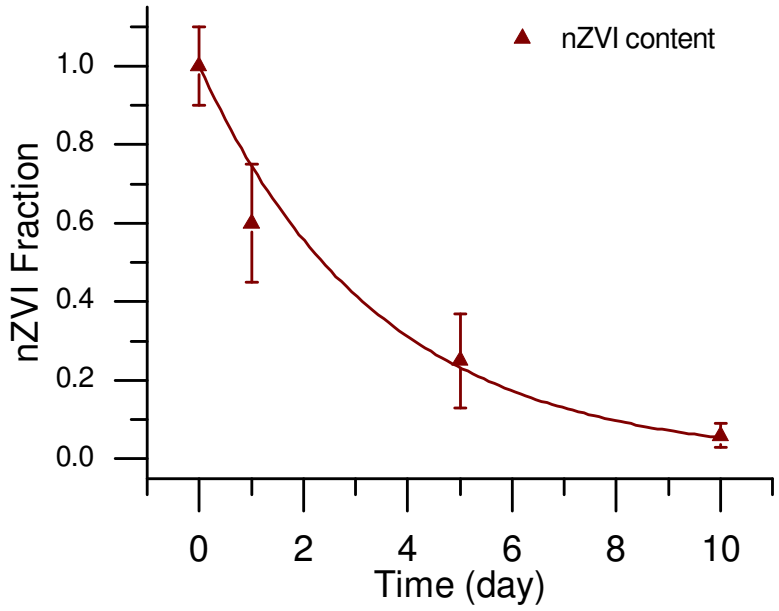

Figure S12. Debromination rate of BDE21 by nZVI/Pd-AC. The data were fitted with the model described by Equation 2. The Y-axis represents the fraction of the moles of BDE 21 in the solid phase and the aqueous phase normalized by the initial moles of BDE 21. It was assumed that the percentage of each compound in the unextracted portion of solid phase is the same as that observed from the extracted portion.

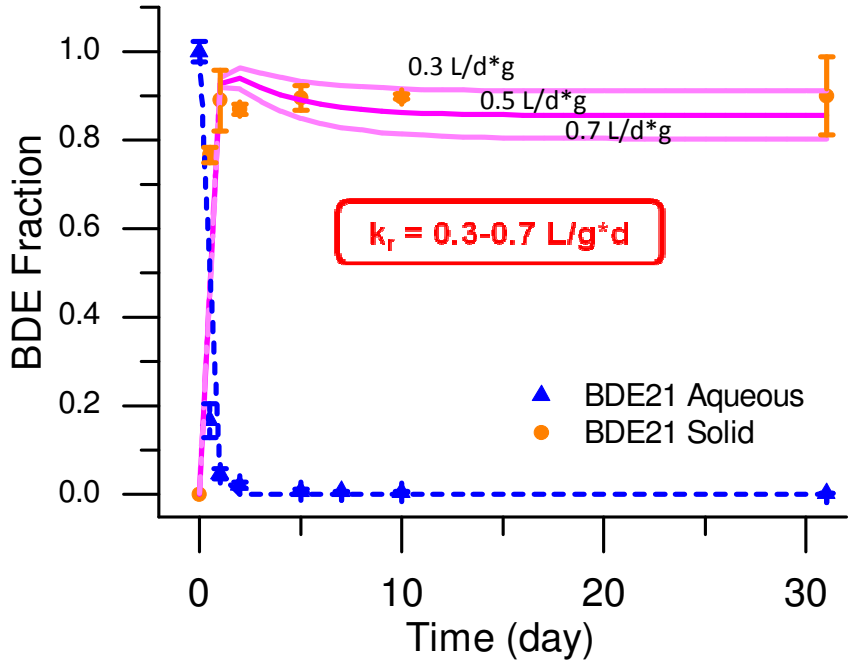

Literature Cited

(1) Zhuang, Y. A.; Ahn, S.; Luthy, R. G. Debromination of polybrominated diphenyl ethers by nanoscale zerovalent iron: Pathways, kinetics, and reactivity. *Environ. Sci. Technol.* **2010**, *44* (21), 8236-8242.

(2) Ghosh, U.; Zimmerman, J. R.; Luthy, R. G. PCB and PAH speciation among particle types in contaminated harbor sediments and effects on PAH bioavailability. *Environ. Sci. Technol.* **2003**, *37* (10), 2209-2217.

(3) Hu, J. W.; Eriksson, L.; Bergman, A.; Jakobsson, E.; Kolehmainen, E.; Knuutinen, J.; Suontamo, R.; Wei, X. H. Molecular orbital studies on brominated diphenyl ethers. Part II - reactivity and quantitative structure - activity (property) relationships. *Chemosphere* **2005**, *59* (7), 1043-1057.